Journal of Solid State Chemistry 285 (2020) 121232

Contents lists available at ScienceDirect

Journal of Solid State Chemistry

journal homepage: www.elsevier.com/locate/jssc

Size, disorder, and charge doping effects in the antiferromagnetic series $Eu_{1-x}A_xGa_4$ (A = Ca, Sr, or La)

Macy Stavinoha [a,*], C.-L. Huang [b], Kasey P. Devlin [c], James C. Fettinger [c], Susan M. Kauzlarich [c], E. Morosan [a,b]

[a] Department of Chemistry, Rice University, Houston, TX, 77005, USA
[b] Department of Physics and Astronomy, Rice University, Houston, TX, 77005, USA
[c] Department of Chemistry, University of California, Davis, CA, 95616, USA

ARTICLE INFO

Keywords:
Antiferromagnetism
Crystal anisotropy
Structural phase transitions
BaAl4

ABSTRACT

$EuGa_4$ hosts a magnetic Eu^{2+} sublattice surrounded by a network of covalently-bound Ga atoms with the $BaAl_4$ structure type (space group $I4/mmm$). In this study, we present the synthesis and characterization of three new single crystal substitutional series EuA_xGa_4 with A = Ca, Sr, or La. X-ray diffraction and resistivity measurements show that Ca substitution induced a structural phase transition from the tetragonal crystal structure at high temperatures to the monoclinic crystal structure ($CaGa_4$ type, space group $C2/m$) at low temperatures and suppressed the antiferromagnetic ordering temperature to 8.8 K for $x = 0.45$. Comparatively, La or Sr substitution maintained the tetragonal crystal structure and suppressed the antiferromagnetic ordering temperatures to 6.7 K and 1.6 K for (A, x) = (La, 0.37) and (Sr, 0.91), respectively. In addition to suppressing the magnetic order, magnetization and specific heat measurements indicate the onset of anisotropic metamagnetic transitions in (La, 0.18), (La, 0.37), and (Sr, 0.63), along with an incommensurate-to-commensurate magnetic transition in (Sr, 0.38). By comparing these effects of doping $EuGa_4$, we show how size, disorder, and charge determine the structure-physical property relations in $EuGa_4$.

1. Introduction

The polar intermetallic compounds of the canonical $BaAl_4$ structure type have been explored to study the bonding in the anionic, covalent sublattice of group 13 or 14 metals and its relationship to the alkali, alkaline earth, or rare earth sublattice [1–4]. The chemical diversity of this group of compounds has ushered in a variety of physical properties that can be designed and tuned, thus providing a template to understand the structure-function relationship. When the cationic sublattice is composed of magnetic rare earth ions, we can particularly examine the role of magnetic Ruderman-Kittel-Kasuya-Yosida (RKKY) interactions on the long-range magnetic order of the compound and how this order might be perturbed by introducing structural, chemical, or electronic variance into the lattice.

$EuGa_4$ is a member of this $BaAl_4$-type structural family ($I4/mmm$, space group #139, $tI10$) and has been investigated for its unique magnetic and electronic properties. The fully divalent Eu ions have shown long-range antiferromagnetic order below 16 K [5,6], and the surprising discovery of a charge density wave below ~130 K was reported with applied pressure of 1.65 GPa [7]. The long-range antiferromagnetic order of the Eu sublattice and its interplay with spin and charge degrees of freedom opens a door to study how perturbing this system affects its physical behaviors. To this aim, chemical substitution in the covalent Ga sublattice with Al, Li, or Mg, or in the magnetic Eu sublattice has been employed. The substituted series $Eu(Ga_{1-x}Al_x)_4$ showed the presence of multiple metamagnetic transitions as x was increased from 0 to 1 [8]. A maximum antiferromagnetic ordering temperature of $T_N = 19$ K coincided with a minimum in the lattice parameter a for $x = 0.5$. When $x = 0.5$ and 1, charge density wave behavior was observed at ambient pressure [8,9]. Interestingly, Li and Mg were successfully incorporated into the Ga sublattice despite their electropositive character similar to Eu^{2+}. The antiferromagnetic ordering temperature was lowered in both the Li- and Mg-substituted compounds [10–12].

While doping the Eu sublattice is an attractive option to study the ground state magnetic order and possibly induce new magnetic phase transitions, it is often chemically less favorable relative to substitutions in the nonmagnetic sublattice. Thus, comparatively little work has been done to determine the effects of substitution in the magnetic Eu sublattice

* Corresponding author.
E-mail address: macylauren@rice.edu (M. Stavinoha).

https://doi.org/10.1016/j.jssc.2020.121232
Received 21 November 2019; Received in revised form 31 January 2020; Accepted 2 February 2020
Available online 6 February 2020

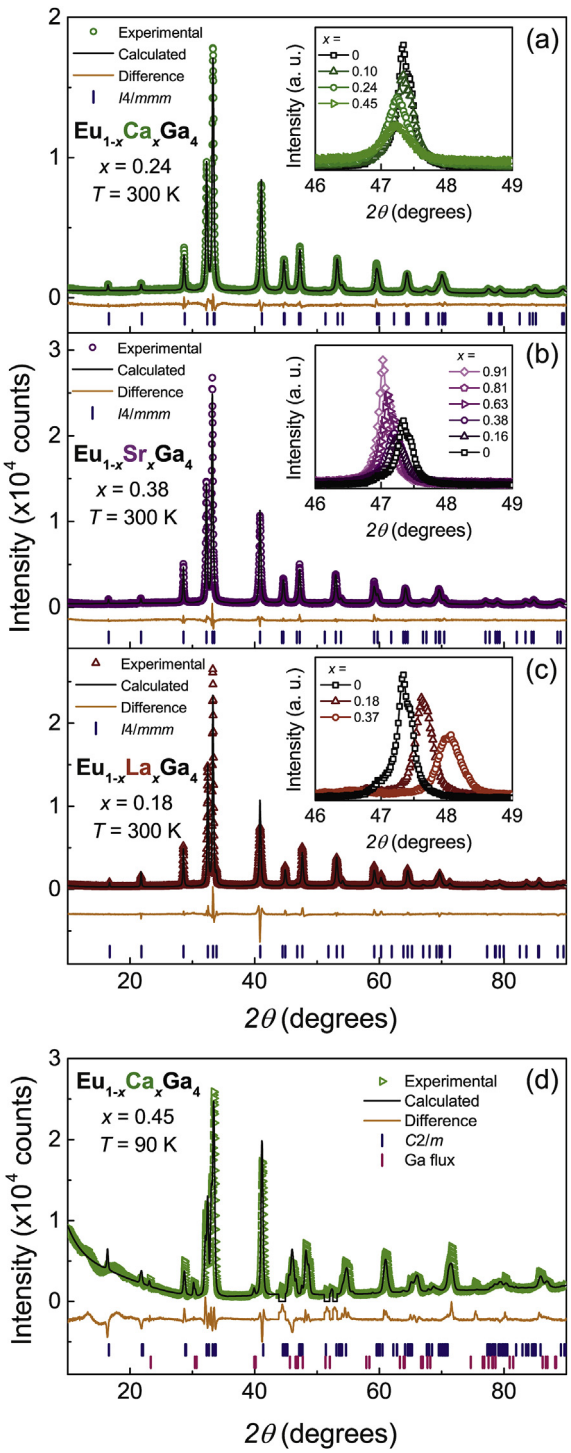

Fig. 1. (a–c) Powder x-ray diffraction at 300 K for EuA_xGa$_4$ with one composition for each A featured in the main panel where A = (a) Ca, (b) Sr, or (c) La. The inset focuses on the change in 2θ for the (015) Bragg peak as x increases in each substitutional series. (d) Powder x-ray diffraction performed at 90 K for $Eu_{1-x}Ca_xGa_4$ with $x = 0.45$ as an example of the structural phase transition from the tetragonal *I4/mmm* to monoclinic *C2/m* space group as the sample was cooled below room temperature.

in EuGa$_4$. Yb was successfully doped into EuGa$_4$, and $Eu_{0.5}Yb_{0.5}Ga_4$ showed a suppressed T_N~ 13 K [13]. With applied pressure, the ordering temperature and the ferromagnetic component of the long-range order increase concomitantly with a shift toward trivalent Eu and Yb ions.

In this study, we systematically investigate the effects of substitution in the Eu sublattice in single crystals of Eu$Eu_{1-x}A_x$Ga$_4$ with A = Ca, Sr or La. While all three dopants are nonmagnetic and therefore dilute the magnetic Eu^{2+} sublattice, Ca and Sr are isovalent to Eu and induce disorder, while trivalent La provides charge doping. Ca, unlike Sr or La, is significantly smaller than Eu and could potentially introduce chemical pressure into the system. We therefore juxtapose the effects of size, disorder, and charge on the magnetic and electronic properties of EuGa$_4$.

2. Experimental methods

Single crystals of EuA_xGa$_4$ with A = Ca, Sr and La were grown using the self-flux technique [8]. Powder x-ray diffraction was performed at ambient or low temperature using a Bruker D8 Advance diffractometer equipped with a MTC-LOWTEMP sample stage using Cu Kα radiation. Rietveld refinements were done using TOPAS software [14]. Single crystal x-ray diffraction was performed using a Bruker Apex II diffractometer or a Rigaku SCX Mini diffractometer with Mo Kα radiation. Integration of raw frame data was done using Bruker Apex II software [15] or Rigaku CrysAlis Pro software [16]. Refinement of the diffraction data was performed using XPREP and ShelXTL software packages [17, 18].

DC magnetic susceptibility measurements were performed using a Quantum Design Magnetic Properties Measurement System. Heat capacity measurements were performed using an adiabatic thermal relaxation technique using a Quantum Design Physical Properties Measurement System (PPMS) equipped with a ^{3}He insert. Temperature-dependent DC/AC resistivity measurements were performed using a PPMS with a typical current i = 2–3 mA with $i||ab$.

Quantitative composition analysis was performed from Electron Probe Micro-Analyser (EPMA) measurements using a JEOL JXA 8530F Hyperprobe equipped with a field emission (Schottky) emitter and five WDS spectrometers. The standards used for element calibration were synthetic GaAs for Ga, and synthetic glasses REE1 and REE3 [19] for Eu and La, respectively. Careful background offsets were selected in order to avoid interferences with other first order x-rays during peak and background measurement (in brackets the lower and upper background offsets, respectively): Ga (−4 mm, +5 mm), Eu (−4 mm, + 5 mm), La (−5 mm, + 6 mm). Average detection limits and standard deviation 1σ (in brackets) are 510 ppm for Ga (0.29%), 470 ppm for Eu (0.46%), and 520 ppm for La (1.68%). In order to avoid the interferences with higher order x-ray lines, Eu and Ga were measured in differential mode, while La was analyzed in integral mode. The ZAF matrix correction was employed for quantification.

3. Results

Single crystals of EuA_xGa$_4$ formed as thin plates with typical dimensions around 2 x 1 x 0.5 mm^3. We used a combination of ambient and low-temperature powder and single crystal x-ray diffraction to determine the structural properties of each reported composition. Powder x-ray diffraction indicates that at T = 300 K, all compounds reported here crystallize with the tetragonal *I4/mmm* space group. A representative powder x-ray diffraction at ambient temperature is displayed for each series in Fig. 1(a–c) with insets showing the change in the (015) Bragg peak as x increases. The tetragonal crystal structure is pictured in Fig. 6(c). Attempts to determine the composition and crystal structure from single crystal diffraction revealed additional information: for A = Sr, T = 173 K single crystal x-ray data confirmed the same tetragonal space group at this temperature, and yielded the doping fractions x for $Eu_{1-x}Sr_xGa_4$. When A = La, the single crystal x-ray free variable refinements confirmed the tetragonal crystal structure, but did not provide consistent values of x, possibly due to the similar electron density of Eu and La ions. Thus, EPMA was used to determine x for the $Eu_{1-x}La_xGa_4$ series. The A = Ca single crystal x-ray refinements at T = 173 K were indicative of a structural phase transition close to this temperature. Therefore additional single crystal x-ray measurements were performed

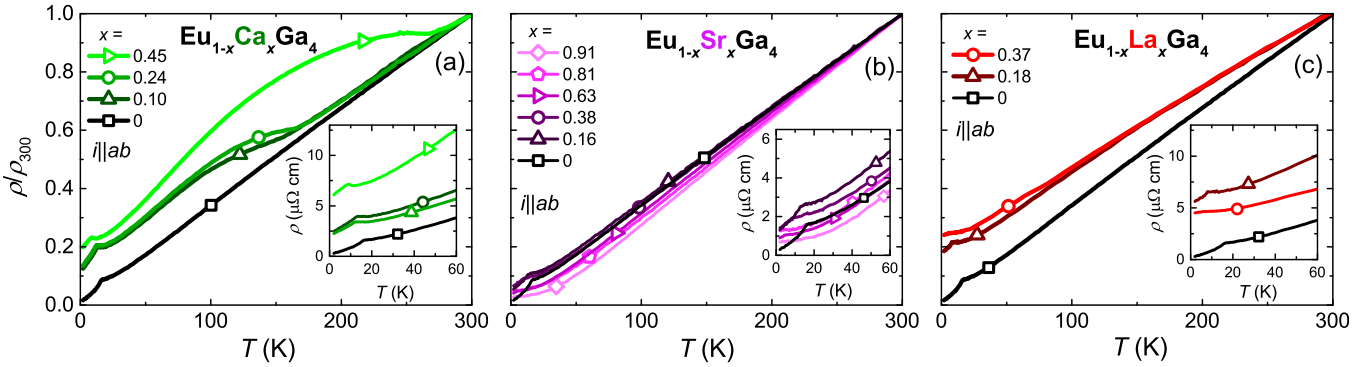

Fig. 2. H = 0 temperature-dependent resistivity scaled by ρ_{300}. Insets show absolute resistivity values at low temperature to emphasize the loss of spin disorder scattering at the antiferromagnetic ordering temperature.

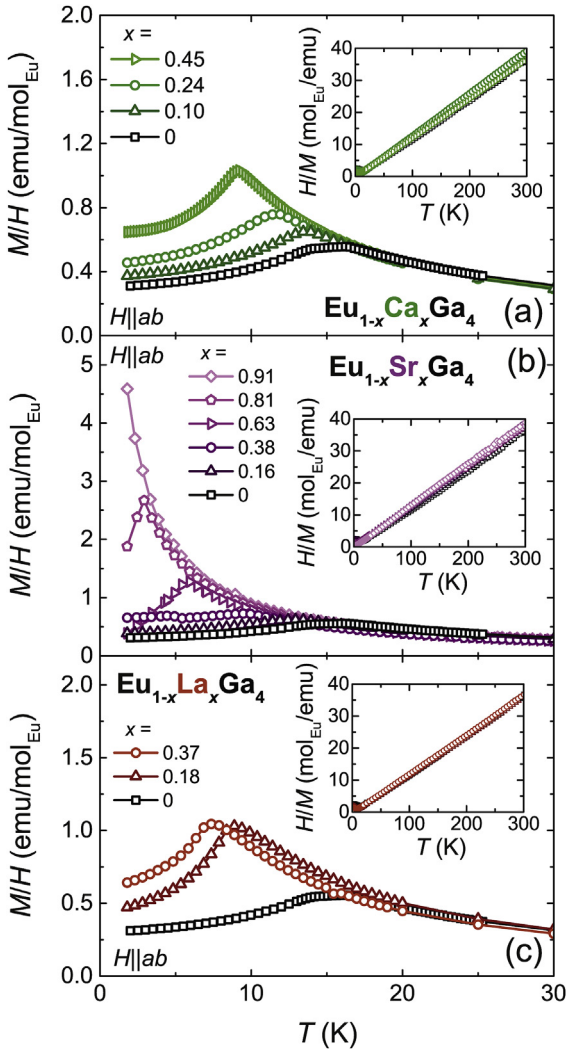

Fig. 3. Temperature-dependent magnetic susceptibility M/H measurements for EuA_xGa_4 with A = Ca (a), Sr (b) or La (c). All measurements were performed with $\mu_0 H \parallel ab$ = 0.1 T. Insets in each main panel show the inverse magnetic susceptibility calculated using the polycrystalline average of the magnetization for all doping fractions.

at T = 300 K, which, as shown below, is far above the structural phase transition identified from these and low temperature (T = 90 K) powder diffraction measurements. Values for x were determined from free variable refinement of the single crystal diffraction data at T = 300 K. All

Table 1
Physical properties of EuA_xGa_4 with A = Ca, Sr, or La obtained from resistivity, magnetization, and specific heat measurements.

***A* = Ca**					
x	0	0.10	0.24	0.45	
T_N (K)	16.2 ± 0.2	13.3 ± 0.9	10.5 ± 0.2	8.8 ± 0.4	
θ_W (K)	8.87	2.08	4.95	1.11	
RRR	62.4	8.04	7.38	5.05	
***A* = Sr**					
x	0.16	0.38	0.63	0.81	0.91
T_N (K)	12.4 ± 1.0	9.2 ± 0.7	5.3 ± 0.4	2.8 ± 0.3	1.6
θ_W (K)	4.20	2.00	0.14	1.54	2.47
RRR	18.3	15.2	24.7	20.5	36.1
***A* = La**					
x	0.18	0.37			
T_N (K)	8.2 ± 0.3	6.7 ± 0.4			
θ_W (K)	5.74	3.34			
RRR	5.4	4.2			

reported $Eu_{1-x}Ca_xGa_4$ samples undergo a transition to the monoclinic $CaGa_4$ structure type ($C2/m$, space group #12, $mS10$), consistent with the report by Bruzzone et al. for $CaGa_4$ [20]. Fig. 1(d) shows powder x-ray diffraction data measured at T = 90 K for A = Ca with x = 0.45 indicating the change in Bragg peak positions as a result of the monoclinic distortion on cooling. For completion, single crystal x-ray data were collected at T = 90 K for one sample in each of the other two series (A = Sr, Eu), which showed that the tetragonal $I4/mmm$ space group is preserved down to this temperature for these two series. Details of the single crystal x-ray refinements and EPMA are summarized in Table 2 and can be obtained as described in [23].

Temperature-dependent electrical resistivity data provide insight into the metallic nature of EuA_xGa_4 and hint at structural and magnetic phase transitions in the series. Fig. 2 shows resistivity scaled at 300 K ρ/ρ_{300} for A = (a) Ca, (b) Sr and (c) La. In $EuGa_4$ (squares), metallic resistivity is indicated by a monotonous resistivity decrease on cooling, followed by a drop at T_N = 16 K signaling the loss of spin-disorder scattering at the onset of antiferromagnetic order [5,6]. Good crystal quality is indicated by the low residual resistivity values $\rho_0 \approx 0.1$ μΩ cm (inset, Fig. 2(a)) and large residual resistivity ratio RRR = $\rho_{300}/\rho_0 \sim$ 5–8. As Ca is substituted for Eu with x = 0.10 (up triangle, Fig. 2(a)), the metallic resistivity at high temperatures precedes, on cooling, a broad peak below $T^* \sim$ 150 K. Similar features are observed in the x = 0.24 (circle) and 0.45 (right triangle) samples at 164 K and 263 K, respectively. We attribute this slight increase in scattering to the onset of the structural phase transition to the monoclinic $C2/m$ space group. This is supported by the comparison of room-temperature versus low-temperature powder and single crystal x-ray diffraction data of all Ca-substituted compounds. As the temperature is further lowered below T^*, the onset of magnetic order is apparent

as a drop in resistivity (inset, Fig. 2(a)). As expected when the magnetic Eu sublattice is diluted with nonmagnetic Ca, T_N decreases with increasing x, while increased disorder induced by the random Eu–Ca mixture is consistent with enhanced ρ_0 and reduced RRR.

By comparison, the A = Sr and La compounds are metallic for all reported concentrations (Fig. 2(b) and (c)), with the ordering temperature decreasing with increasing x. As was the case for A = Ca, the transport behavior when A = La shows increased scattering in the scaled resistivity at low temperature as x increases, which is consistent with greater disorder introduced through substitution. However, A = Sr shows only a very small change in the scaled residual resistivity as x varies, likely due to the similarity in size between the Eu^{2+} and Sr^{2+} ions. The magnetic phase transition observed up to x = 0.63 is marked, as expected, by a drop in resistivity due to loss of spin disorder scattering.

To better understand the nature of the magnetic order in these compounds, magnetic susceptibility measurements with $\mu_0 H \parallel ab = 0.1$ T are shown in Fig. 3. In the $Eu_{1-x}Ca_xGa_4$ systems (top panel), a cusp in the magnetic susceptibility M/H indicates the onset of antiferromagnetic order. The ordering temperature T_N was determined from the peak in $d(MT)/dT$ [21] to be 15.9 K when x = 0, and is suppressed with increasing x down to T_N = 8.4 K for x = 0.45. The insets in Fig. 3 show the inverse magnetic susceptibility H/M up to 300 K. All members of the $Eu_{1-x}Ca_xGa_4$ series follow Curie-Weiss behavior with measured effective moments p_{eff}^{exp} = 7.93, 7.77 and 8.14 for x = 0.10, 0.24, and 0.45,

Table 2
Crystallographic parameters obtained from single crystal x-ray refinements for $Eu_{1-x}A_xGa_4$ when A = Ca, Sr, or La [23].

A = Ca					
x[a]	0[b]	0.10	0.24	0.45	
Temperature (K)	90	300	300	90 (300)	
Space group	*I4/mmm*	*I4/mmm*	*I4/mmm*	*C2/m* (*I4/mmm*)	
a (Å)	4.3904(7)	4.3988(2)	4.38699(15)	6.193(2) (4.3896(2))	
b (Å)	4.3904(7)	4.3988(2)	4.38699(15)	6.166(2) (4.3896(2))	
c (Å)	10.6720(18)	10.6838(13)	10.6715(9)	6.143(2) (10.7113(16))	
V (Å^3)	205.71(7)	206.73(3)	205.38(2)	204.22(13) (206.39(4))	
β (degrees)	90	90	90	119.479(5) (90)	
Absorption coefficient (mm^{-1})	40.64	39.08	37.41	34.77 (34.35)	
Measured reflections	1656	1551	1741	1294 (1556)	
Independent reflections	137	130	129	383 (129)	
R_{int}	0.036	0.044	0.028	0.039 (0.045)	
Goodness of fit on F^2	1.23	1.24	1.28	1.16 (1.25)	
$R_1(F)$ for $F_o^2 > 2\sigma(F_o^2)^c$	0.014	0.022	0.013	0.037 (0.021)	
$wR_2(F_o^2)^d$	0.037	0.050	0.032	0.098 (0.045)	
Extinction coefficient	0.0127(11)	0.0017(9)	0.0128(9)	0.0054(16) (0.0074(11))	
A = Sr					
x[a]	0.16	0.38	0.63	0.81	0.91
Temperature (K)	173	173	173	90	173
Space group	*I4/mmm*	*I4/mmm*	*I4/mmm*	*I4/mmm*	*I4/mmm*
a (Å)	4.4225(3)	4.4126(2)	4.3850(2)	4.4221(8)	4.43728(17)
c (Å)	10.7286(17)	10.6987(14)	10.6039(16)	10.713(2)	10.7394(11)
V (Å^3)	209.84(4)	208.31(3)	203.89(4)	209.50(9)	211.45(3)
Absorption coefficient (mm^{-1})	39.51	39.33	39.64	38.20	37.64
Measured reflections	1761	1777	1737	1788	1828
Independent reflections	133	133	133	137	135
R_{int}	0.098	0.053	0.057	0.023	0.045
Goodness of fit on F^2	1.12	1.11	1.22	1.24	1.16
$R_1(F)$ for$F_o^2 > 2\sigma(F_o^2)^c$	0.032	0.018	0.023	0.013	0.016
$wR_2(F_o^2)^d$	0.070	0.028	0.032	0.027	0.027
Extinction coefficient	–	–	–	0.0077(6)	0.0019(4)
A = La					
x[e]	0.18	0.37			
Temperature (K)	90	173			
Space group	*I4/mmm*	*I4/mmm*			
a (Å)	4.4045(8)	4.39966(16)			
c (Å)	10.5743(19)	10.4173(8)			
V (Å^3)	205.14(8)	201.65(2)			
Absorption coefficient (mm^{-1})	40.23	39.62			
Measured reflections	1734	1754			
Independent reflections	135	129			
R_{int}	0.024	0.029			
Goodness of fit on F^2	1.26	1.20			
$R_1(F)$ for $F_o^2 > 2\sigma(F_o^2)^c$	0.009	0.013			
$wR_2(F_o^2)^d$	0.020	0.028			
Extinction coefficient	0.0049(4)	0.0040(5)			

[a] From free variable refinement in single crystal XRD.
[b] Data reproduced from Ref. [8].
[c] $R_1 = \sum||F_o| - |F_c||/\sum|F_o|$
[d] $wR_2 = [\sum[w(F_o^2 - F_c^2)^2]/\sum[w(F_o^2)^2]]^{1/2}$
[e] From EPMA.

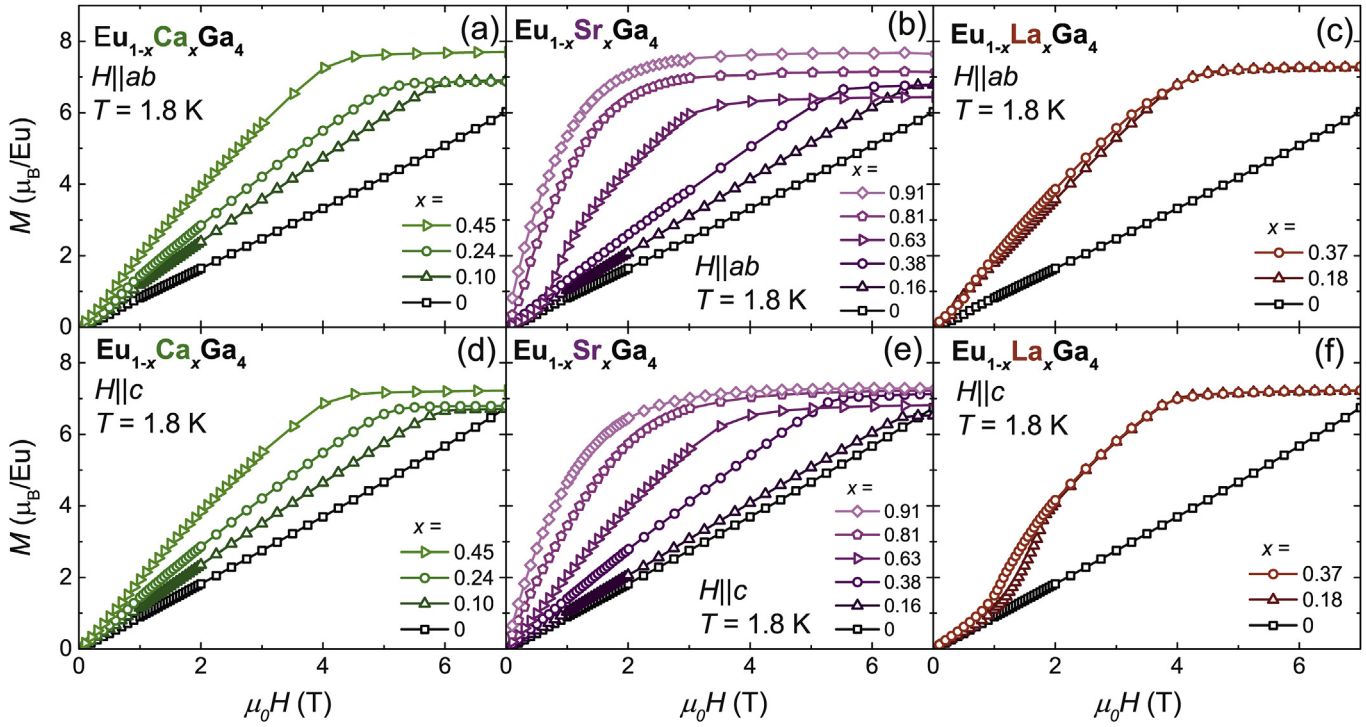

Fig. 4. Field-dependent magnetization measurements with $H\|\|ab$ (a–c) and $H\|\|c$ (d–f). All measurements were performed at 1.8 K.

respectively, which are close to $p_{eff}^{calc} = 7.94$ and hence indicate divalent Eu ions. All reported H/M measurements were calculated from the polycrystalline average of the magnetization $M_{ave} = \frac{1}{3}(2M_{ab}+M_c)$.

In $Eu_{1-x}Sr_xGa_4$ shown in Fig. 3(b), we can trace the suppression of T_N across a larger range of substitution from $x = 0.16$ to 0.91. We observe the cusp consistent with the onset of antiferromagnetic order down to 2.5 K in $x = 0.81$. Specific heat measurements performed down to 0.5 K (shown below) indicate that $x = 0.91$ orders at 1.6 K. Interestingly, $x = 0.38$ is the only composition in this series that undergoes a second magnetic phase transition, consistent with an incommensurate-to-commensurate magnetic transition at 4.0 K. This transition is indeed confirmed in specific heat measurements (below). H/M data in the inset provide p_{eff}^{exp} values of 7.92, 7.85, 8.00, 7.97, and 7.81 for $x = 0.16$, 0.38, 0.63, 0.81, and 0.91, respectively, affirming fully divalent Eu ions.

By comparison, $Eu_{1-x}La_xGa_4$ also undergoes antiferromagnetic order that is suppressed with increasing La substitution as shown in Fig. 3(c). In this case, T_N is suppressed to $T_N = 7.9$ K when $x = 0.18$ and then to 6.4 K when $x = 0.37$. Temperature-dependent H/M in the inset shows Curie-Weiss behavior with $p_{eff}^{exp} = 8.1$ for both $x = 0.18$ and 0.37, confirming that only divalent Eu ions are present. The maximum x values were dictated by the solubility limit of A is $EuGa_4$. A summary of the Weiss temperatures θ_W (determined from the Curie-Weiss fit to H/M) and magnetic ordering temperatures determined from $d(MT)/dT$ and specific heat measurements (shown below) is given with the error associated between the two measurements in Table 1.

To complement temperature-dependent M/H measurements, field-dependent magnetization measurements are shown in Fig. 4. Measurements with $H \| ab$ are shown in (a-c), and with $H \| c$ in (d-f). All measurements were performed at $T = 1.8$ K, which is within the antiferromagnetic state for all compounds except $x = 0.91$ in $Eu_{1-x}Sr_xGa_4$, which orders below this temperature. In all systems, magnetic saturation is achieved at $\mu_{sat} = 7\ \mu_B/Eu^{2+}$ close to $\mu_0 H = 7$ T. The only exception is $EuGa_4$ (squares), which is approaching saturation but may only reach 7 μ_B just above the maximum field available for these measurements (7 T). A number of metamagnetic transitions occur anisotropically throughout these series. In $Eu_{1-x}Sr_xGa_4$, a metamagnetic transition can be observed only in $x = 0.63$ when $\mu_0 H = 0.8$ T is applied along the ab plane (Fig. 4(b)), while in $Eu_{1-x}La_xGa_4$ two or more metamagnetic transitions are apparent for $x = 0.18$ and 0.37 at $\mu_0 H = 1.75$ T and 1.10 T, respectively, only with $H \| c$ (Fig. 4(f)).

Temperature-dependent specific heat measurements C_P with $H = 0$ were performed on each series and are reported in Fig. 5. In $Eu_{1-x}Ca_xGa_4$ (Fig. 5(a)), the ordering temperatures of the antiferromagnetic transitions are suppressed down to a minimum $T_N = 9.2$ K in $x = 0.45$. No additional phase transitions are observed in this temperature range. The smooth suppression of T_N in $Eu_{1-x}Sr_xGa_4$ with increasing x is shown in Fig. 5(b). We observe that magnetic order is attained in every composition, with $x = 0.91$ hosting the lowest T_N of 1.6 K. Additionally, C_P measurements confirm the presence of an incommensurate-to-commensurate magnetic phase transition only in $x = 0.38$ as noted in temperature-dependent M/H measurements. $C_P(T)$ reveals that this transition is actually composed of two peaks, one occurring at 5.0 K followed by the second at 4.7 K. Lastly, the magnetic ordering transitions in $Eu_{1-x}La_xGa_4$ (c) are also supported by specific heat measurements. These measurements furthermore reveal that each phase transition in $x = 0.18$ and $x = 0.37$ has a small "shoulder" indicating the close proximity of two phase transitions at T_N, with the lowest ordering temperature suppressed to 7.0 K in the latter composition.

4. Discussion and conclusions

$EuGa_4$ has proven to be a useful template for studying the effects of doping on its magnetic, electronic, and crystallographic properties. We have demonstrated here the changes introduced in its transport, magnetic order, and crystallography when Eu is substituted with the smaller Ca ion, the isovalent Sr ion, or the trivalent La ion. In Fig. 6(a), we compare the effect of the Ca doping fraction x on the critical temperature T^* of the structural phase transition (left axis, stars), the ordering temperature T_N (left axis, open triangles), and the volume of the unit cell at 300 K (right axis, closed triangles). Introducing a fraction of only 0.10 Ca ions is sufficient to bring about a structural phase transition at $T^* = 150$

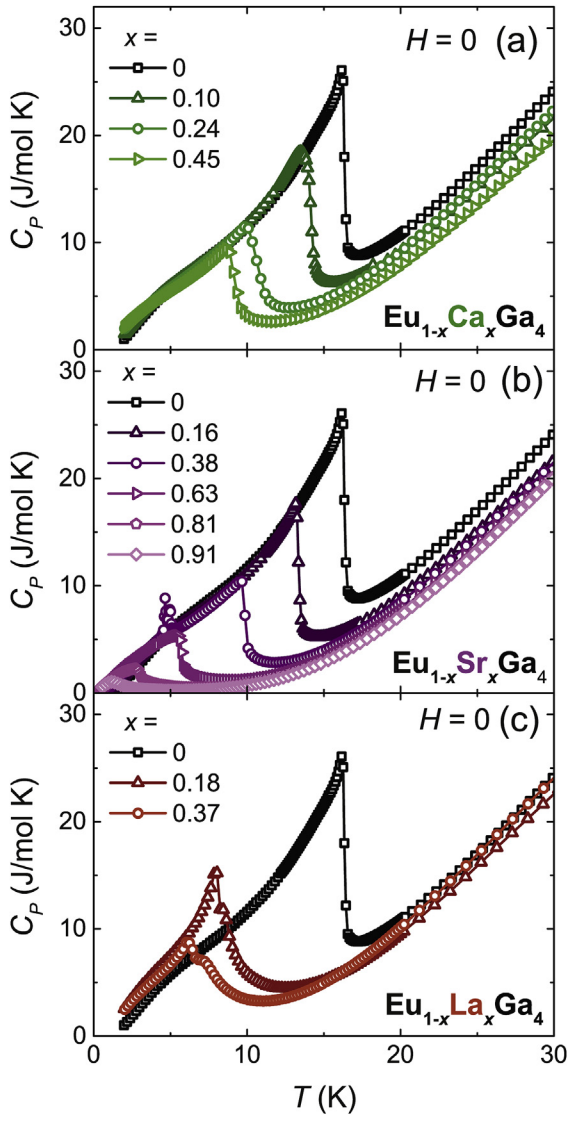

Fig. 5. Temperature-dependent specific heat measurements with $H = 0$ for EuA_xGa_4 where A = (a) Ca, (b) Sr, or (c) La. When A = Sr and $x = 0.38$, a double-peaked phase transition can be observed ~5 K.

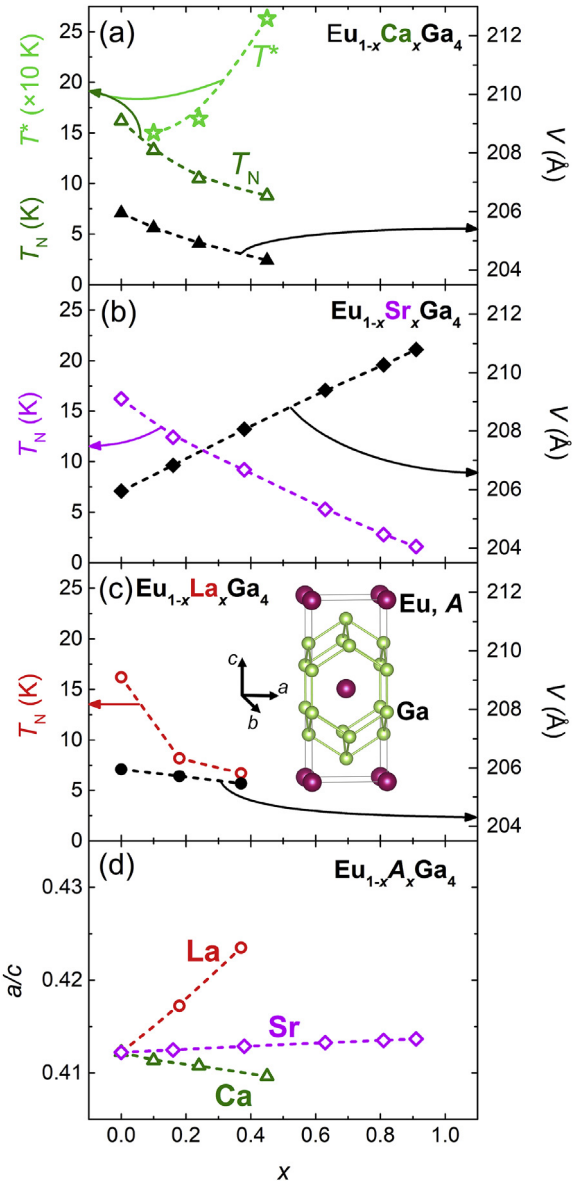

Fig. 6. (a) Left axis, stars: The critical temperature T^* of the structural phase transition from the tetragonal to monoclinic crystal system in $Eu_{1-x}Ca_xGa_4$. (a–c) Left axis, open symbols: The antiferromagnetic ordering temperature T_N of the Ca, Sr or La substitutional series as a function of the doping fraction x. Right axis, closed symbols: (a–c) The volume of the tetragonal unit cell at 300 K as a function of the doping fraction x. Unit cell volume at 300 K was determined using powder x-ray diffraction refinements. The tetragonal $I4/mmm$ unit cell is shown as an inset in (c). (d) Ratio of a and c lattice parameters for A = La (red circles), Sr (purple diamonds), or Ca (green triangles) as determined by powder x-ray diffraction refinements. (For interpretation of the references to colour in this figure legend, the reader is referred to the Web version of this article.)

K, and modestly contracting the unit cell to 99.2% of its original volume steeply raises T^* to 263 K. This indicates that the Eu sublattice is quite resistant to incorporation of smaller ions into the site while maintaining the tetragonal structure. This is supported by studies done by Fedorchuk et al. showing that smaller Li or Mg ions preferentially occupy the Ga sublattice despite their chemical similarity to Eu [12].

Remarkably, the long-range magnetic order is maintained in $Eu_{1-x}Sr_xGa_4$ even when $x = 0.91$, suggesting the persistence of RKKY interactions between Eu ions. At this degree of Sr substitution, the unit cell volume increases to 102% of its original volume, indicating that the Eu sublattice may be significantly more hospitable to larger ions as opposed to smaller ones. This is also supported by comparing the residual resistivity ratio RRR of the Sr-substituted series to that of the La- or Ca-substituted series. While the RRR for the La-substituted series ranges from 5.4 to 4.2 and for the Ca-substituted series from 5.1 to 8.0, the Sr-substituted series hosts high RRR values between 15.2 and 36.1. These high RRR values in $Eu_{1-x}Sr_xGa_4$ concomitant with increasing the unit cell volume suggest that the larger substituent ion imparts very few effects from disorder into the system and opens a door for substituting a variety of larger ions with different charges, to explore their role in affecting the long-range magnetic order and structural stability in the EuA_xGa_4 series.

Substituting trivalent La into the Eu sublattice suppresses T_N more rapidly than Ca or Sr with little change in the volume of the unit cell as demonstrated in Fig. 6(c). When x reaches 0.37, T_N achieves a minimum of 6.7 K ± 0.3 K. However, further incorporation of La^{3+} results in the formation of a secondary orthorhombic phase (not shown), indicating that charge may be a contributing factor to the stability of the crystal structure. When we compare this to Sr^{2+} substitution with $x = 0.38$ (b), T_N is suppressed to a lesser degree to 9.2 K ± 0.7 K, despite the fact that this suppression is accompanied by an increase of the unit cell volume to 101% of its original volume. Thus, charge substitution seems to play a role in suppressing T_N through means in addition to diluting the moment,

along with instigating anisotropic magnetic phase transitions in $Eu_{1-x}La_xGa_4$, as suggested by the metamagnetic transitions observed in $x = 0.18$ and 0.37 when $H \parallel c$.

In summary, we report three new substitutional series in the magnetic Eu sublattice of $EuGa_4$. In $Eu_{1-x}Ca_xGa_4$, a structural phase transition to the monoclinic crystal structure is traced as a function of x, likely due to the smaller ionic radii of Ca^{2+} compared to Eu^{2+}. When $A = La^{3+}$ in EuA_xGa_4, the charge substitution rapidly reduces the antiferromagnetic ordering temperature to a minimum of 6.7 K ± 0.3 K but encounters secondary phase formations as x increases beyond 0.37. By comparison, when $A =$ Sr the antiferromagnetic ordering temperature smoothly decreases to 1.6 K when $x = 0.91$ and 0 in $SrGa_4$ [22] indicating the persistence of RKKY interactions underlying the magnetic order in $EuGa_4$. Additionally, the unit cell is able to be expanded to 102% of its original size with disorder introducing minimal effects on the physical properties on the system as evidenced by high RRR values throughout the $A =$ Sr series. To further explore the effects of charge and size on the magnetic properties of $EuGa_4$, additional A ions with larger ionic radii and +1 valence states such as Na, K, or Rb could act as a valuable counterpart to the current study.

Declaration of competing interest

The authors declare that they have no known competing financial interests or personal relationships that could have appeared to influence the work reported in this paper.

CRediT authorship contribution statement

Macy Stavinoha: Investigation, Formal analysis, Writing - original draft. **C.-L. Huang:** Methodology, Formal analysis. **Kasey P. Devlin:** Formal analysis. **James C. Fettinger:** Formal analysis. **Susan M. Kauzlarich:** Supervision, Project administration. **E. Morosan:** Supervision, Project administration, Writing - original draft.

Acknowledgements

The use of the EPMA facility in the Department of Earth Science, Rice University is kindly acknowledged. MS, CLH, and EM acknowledge support from the Gordon and Betty Moore Foundation EPiQS initiative through grant GBMF 4417. This work was funded in part by a QuantEmX travel grant from ICAM and the Gordon and Betty Moore Foundation through Grant GBMF5305 to MS. The work performed at University of California, Davis was supported by NSF-DMR-1709382.

References

[1] U. Häussermann, S. Amerioun, L. Eriksson, C.-S. Lee, G.J. Miller, J. Am. Chem. Soc. 124 (2002) 4371.
[2] O. Pecher, B. Mausolf, V. Peters, K. Lamberts, A. Korthaus, F. Haarmann, Chem. Eur J. 22 (2016) 17833.
[3] J.K. Burdett, G.J. Miller, Chem. Mater. 2 (1990) 12.
[4] C. Zheng, R. Hoffmann, Z. Naturforsch. B Chem. Sci. 41 (1986) 292.
[5] S. Bobev, E.D. Bauer, J. Thompson, J.L. Sarrao, J. Magn. Magn Mater. 277 (2004) 236.
[6] M. Yogi, S. Nakamura, N. Higa, H. Niki, Y. Hirose, Y. Ōnuki, H. Harima, J. Phys. Soc. Jpn. 82 (2013), 103701.
[7] A. Nakamura, T. Uejo, F. Honda, T. Takeuchi, H. Harima, E. Yamamoto, Y. Haga, K. Matsubayashi, Y. Uwatoko, M. Hedo, et al., J. Phys. Soc. Jpn. 84 (2015) 124711.
[8] M. Stavinoha, J.A. Cooley, S.G. Minasian, T.M. McQueen, S.M. Kauzlarich, C.-L. Huang, E. Morosan, Phys. Rev. B 97 (2018), 195146.
[9] S. Shimomura, H. Murao, S. Tsutsui, H. Nakao, A. Nakamura, M. Hedo, T. Nakama, Y. Ōnuki, J. Phys. Soc. Jpn. 88 (2018), 014602.
[10] A.K. Iyer, L. Balisetty, S. Sarkar, S.C. Peter, J. Alloys Compd. 582 (2014) 305.
[11] T.-S. You, G.J. Miller, Z. Anorg. Allg. Chem. 634 (2008) 2845.
[12] A. Fedorchuk, Y. Prots, Y. Grin, Z. Kristallogr. N. Cryst. Struct. 220 (2005) 317.
[13] G. Loula, R. Dos Reis, D. Haskel, F. Garcia, N. Souza-Neto, F. Gandra, Phys. Rev. B 85 (2012), 245128.
[14] TOPAS, Version 4.2, Bruker AXS, Karlsruhe, Germany, 2009.
[15] APEX Suite of Crystallographic Software, APEX 2 Version 2014.9; SAINT, Version 8.34a; SADABS, Version 2014/5; Bruker AXS Inc.: Madison, WI, U.S.A.
[16] P.R.O. CrysAlis, Rigaku Oxford Diffraction, Yarnton, England, 2015.
[17] G.M. Sheldrick, Acta Crystallogr. C: Struct. Chem. 71 (2015) 3.
[18] SHELXL-2014, Program for the Refinement of Crystal Structures, George M. Sheldrick, University of Göttingen, Germany, 2014.
[19] E. Jarosewich, L. Boatner, Geostand. Newsl. 15 (1991) 397.
[20] G. Bruzzone, M. Fornasini, F. Merlo, J. Less Common Met. 154 (1989) 67.
[21] M.E. Fisher, Phil. Mag. 7 (1962) 1731.
[22] H. Niki, N. Higa, S. Nakamura, H. Kuroshima, T. Toji, M. Yogi, A. Nakamura, M. Hedo, T. Nakama, Y. Ōnuki, et al., Hyperfine Interact. 231 (2015) 57.
[23] FIZ Karlsruhe, 76344 Eggenstein-Leopoldshafen, Germany [fax: (+49)7247-808-666; email: crysdata@fiz-karlsruhe.de], on quoting the deposition numbers CSD-1966356, -1966357, -1966358, -1966359, -1966360, -1966361, -1966362, -1966363, -1966364, -1966365, and -1897831.